International Symposium
On Turbulence and Shear Flow
Phenomena (TSFP-8)
August 28 - 30, 2013 Poitiers, France

SPATIO-TEMPORAL 3D CORRELATIONS OF FLUCTUATING PRESSURE AND VELOCITY IN A HIGH REYNOLDS NUMBER TURBULENT BOUNDARY LAYER

Yoshitsugu Naka
Department of Mechanical and Aerospace Engineering
Tokyo Institute of Technology
2-12-1 Ookayama, Meguro-ku, Tokyo 152-8550, Japan
ynaka@navier.mes.titech.ac.jp

Sébastien Coudert, Jean-Marc Foucaut, Michel Stanislas
Laboratoire de Mécanique de Lille
Boulevard Paul Langevin, 59655 Villeneuve d'Ascq, France
michel.stanislas@ec-lille.fr

ABSTRACT

In the present study, we developed a new experimental setup for the simultaneous measurements of the fluctuating pressure and the three velocity components in a turbulent boundary layer. A quantitative measure of the extension of the space-time pressure-velocity correlations is given based on their reconstructed 3D distributions. The correlations of the fluctuating pressure and each three velocity components exhibit characteristic behavior: the pressure-streamwise velocity correlations show the inclined elongated shape and have extensions approximately 5-6δ, while the pressure-wall normal velocity correlations are more localized with an extension of 0.3δ and with an inclination of roughly 45° at the pressure reference points close to the wall. The pressure-spanwise velocity correlations show the distribution evoking a representation of the streamwise vortical structures with the size of the order of the boundary layer thickness and the meandering of them.

INTRODUCTION

Quasi-coherent organized motions in the incompressible wall bounded turbulent flows have extensively been investigated. Some distinctive structures are well defined, e.g., near-wall low-speed/high-speed streaks, sweep/ejection motions, hairpin vortices and large-scale bulges, and such structures contribute to correlated pressure and velocity fluctuations. It is now known that structures typically larger than 3δ, called *hairpin packets*, carry a significant fraction of the turbulent kinetic energy and Reynolds stress (Adrian, 2007). Moreover, very long *superstructures* of the streamwise velocity component (more than 20δ) were also reported from atmospheric boundary layer measurements by Hutchins & Marusic (2007). Such *hairpin packets* and *superstructures* are important features of near wall turbulence, but their relation to the pressure fluctuations, is still an open question.

From a statistical point of view, the large structures can be observed in the two-point correlations. Experimental evidences from hot-wire data show that in wall bounded flows, the longitudinal correlation has substantially longer tail than the transverse one (Kovasznay *et al.*, 1970). Recently, Foucaut *et al.* (2011) visualized the three-dimensional shape of the two-point velocity correlations in a turbulent boundary layer, and the correlation of streamwise velocity shows an elongated ellipsoidal shape in the streamwise direction, inclined to the wall at an angle of approximately 10°. Tutkun *et al.* (2009) evaluated the space-time correlations of the streamwise velocity component from the data of a rake of 143 single hot-wire probes, and found that the correlation spreads approximately 7 to 8δ/U_e in time. It is considered that the elongated shape of two-point correlations of streamwise velocity corresponds to the large scale structures.

The pressure fluctuations in incompressible flows are closely linked with the vortex structures. The pressure at one arbitrary point is affected by the whole flow domain as a solution of a Poisson equation, and the pressure fluctuations play a significant role in the transport of the turbulent kinetic energy and Reynolds stresses. Since an appropriate measurement technique has not yet been available for the fluctuating pressure in the vicinity of the wall (not at the wall), experimental studies of the pressure fluctuation in turbulent near wall flows are limited. Difficulty is mainly caused by the fact that the turbulent pressure fluctuations are subtle, and are easily distorted by the ambient noise and probe intrusion, especially adjacent to the wall. Tsuji *et al.* (2007) made a first attempt of measurements of the pressure fluctuations in a turbulent boundary layer by a small static pressure probe. They investigated fundamental statistical quantities such as the mean, r.m.s. and power spectra of pressure fluctuations, and their scaling law.

In the present study, in order to try to link these coherent motions in the turbulent boundary layer to the pressure fluctuations at the wall and in the field, we developed a new experimental setup for the simultaneous measurement of the fluctuating pressure and the three velocity components so that the space-time pressure-velocity correlations in a turbulent boundary layer can be investigated. The pressure at

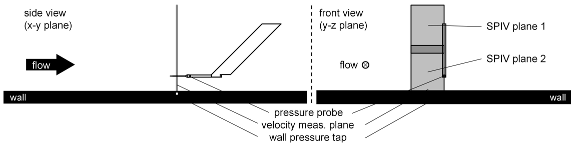

Figure 1. Arrangement of pressure probe, wall pressure tap and stereo PIV plane.

two points: one at the static pressure holes of a probe whose distance from the wall can be adjusted, and another pressure tap on the wall, is captured together with a stereo PIV plane which is arranged perpendicular to the wall and to the mean flow direction. Our target is to reveal how the pressure-velocity correlation is linked to the large-scale structure, and to give a quantitative measure of the extension of the space-time pressure-velocity correlations.

EXPERIMENT

Simultaneous measurements of the fluctuating pressure and velocity were performed in a closed-loop turbulent boundary layer wind-tunnel at Laboratoire de Mécanique de Lille having a cross section of 1 m $\times$ 2 m and a 21.6 m long development section. An (x, y, z) Cartesian coordinate system is defined for the streamwise, wall-normal and spanwise directions respectively. The origin is set at the center of the wall pressure hole which is located in the spanwise plane of symmetry of the wind-tunnel section and at 18 m from the contraction outlet. The free stream velocity U_e was regulated at 3 m/s, 5 m/s and 10 m/s with a stability of 0.5% giving Reynolds numbers based on the momentum thickness θ and U_e, of $Re_\theta = 7300$, 10000 and 18000.

The velocity components u, v and w are defined along the x, y and z directions. The superscript "$+$" refers to the wall unit normalization by u_τ and ν (where u_τ is the wall shear stress and ν is the kinematic viscosity). The characteristics of the boundary layer are described in Carlier & Stanislas (2005). A schematic of the experiment is presented in figure 1. The fluctuating pressure signals at two points: the wall and an arbitrary transverse position were captured, and the field of three velocity components right close to the pressure holes was measured.

Three 1/4-inch microphones (B&K 4938) were installed in the wind-tunnel. Microphone #1 with the pressure probe was attached to the traversing system, microphone #2 was mounted on the wall, and microphone #3 with a nose cone was fixed in the free stream. The signals were recorded at 40 kHz, and the Q-switch signals of the laser were simultaneously recorded for synchronization.

A static pressure probe similar to Naka *et al.* (2006) was used for the present experiment. The pressure probe consists of the tip, pipe and connecting part to the microphone. The outer diameter of the stainless-steel pipe is 1.0 mm and the thickness is 0.05 mm. Two 0.4 mm diameter holes are opened with an angle of 180° at 19.5 mm from the tip. Consequently, the present pressure probe has a measurement volume of $0.4 \times 0.4 \times 1.0$ mm^3 in x-y-z directions. The pressure probe was fixed to a streamlined swept back shape support of a traversing system. The wall pressure tap has a 0.5 mm diameter hole drilled with an inclination angle of 22° in spanwise direction.

The transfer function of the pressure measurement system is taken into account to recover faithful time series of the pressure fluctuation. The signal to noise ratio of the pressure signal was enhanced by a Wiener noise canceller which was implemented with the signals of free stream microphone #3.

Table 1. Wall normal positions of the pressure probe at $Re_\theta = 10000$.

pos.	y_p [mm]	$y_p{}^+$	y_p/δ
(a):	0	0	0
(b):	3.8	48	1.36×10^{-2}
(c):	4.5	56	1.61×10^{-2}
(d):	9.3	117	3.32×10^{-2}
(e):	18.9	237	6.75×10^{-2}
(f):	38.1	477	1.36×10^{-1}
(g):	76.5	959	2.73×10^{-1}
(h):	153.3	1921	5.48×10^{-1}
(i):	230.1	2883	8.22×10^{-1}
(j):	306.9	3846	1.10

As depicted in figure 1, two stereo PIV planes were arranged in $y-z$ plane and were placed side by side in the wall normal direction to cover the whole boundary layer thickness with a good spatial resolution. A 250 mJ/pulse Nd:YAG laser (BMI 5000) was used for illumination. The scattered light from particles were captured by 4 CCD cameras with 2k $\times$ 2k pixels (Hamamatsu C9300) through Nikon 105 mm lenses. The aperture f/8 gave a diffraction spot of approximately 2 pixels. These cameras were mounted in the Scheimpflug condition (Willert, 1997) and the viewing angle and distance between two cameras were 45° and 1.37 m, respectively. For seeding, Poly-Ethylene Glycol particles whose diameter was about 1 μm were generated by a smoke-generator. Each stereo PIV plane had 16 $\times$ 11 cm field of view, and the combined field of 31 cm $\times$ 11 cm was obtained with a small overlap. The sampling rate of stereo PIV was 4 Hz. The two light sheets are slightly separated in x direction (approximately 0.75 mm) to obtain better correlation; note that the light sheet thickness is about 1.85 mm. The time separation between two exposures was optimized: Δt = 250 μs, 150 μs and 75 μs for 3 m/s, 5 m/s and 10 m/s in order to get a maximum displacements of 10 pixels.

The PIV analysis was performed by a standard multi-pass FFT-based cross-correlation method with integer shift of both windows. A 1-D Gaussian peak fitting algorithm was used for the sub-pixel displacement determination. Three passes with different window sizes were used. The interrogation window size of the final pass was 26 $\times$ 39 pixel^2. The physical size of the interrogation window was 2.24 mm $\times$ 2.21 mm in y and z. The velocity was computed at grid points within 1 mm $\leq y \leq$ 308 mm and -0.5 mm $\leq z \leq$ 110 mm. The number of grid points in y and z is 615 and 222 respectively for the combined field, and 45 points were overlapped in y direction. The PIV overlap ratio was 77%. The Soloff method (Soloff *et al.*, 1997) was used to reconstruct the three velocity components. From a set of calibration and stereo PIV particle images, the misalignment between the light sheet and the calibration plane was compensated by the technique described in Coudert & Schon (2001).

Each run of simultaneous measurement was repeated for the 9 different wall normal positions of the pressure probe given in table 1. The number of valid realizations of velocity field is 10 000 for each run. This corresponds to pressure recording during 2 500 s at each position.

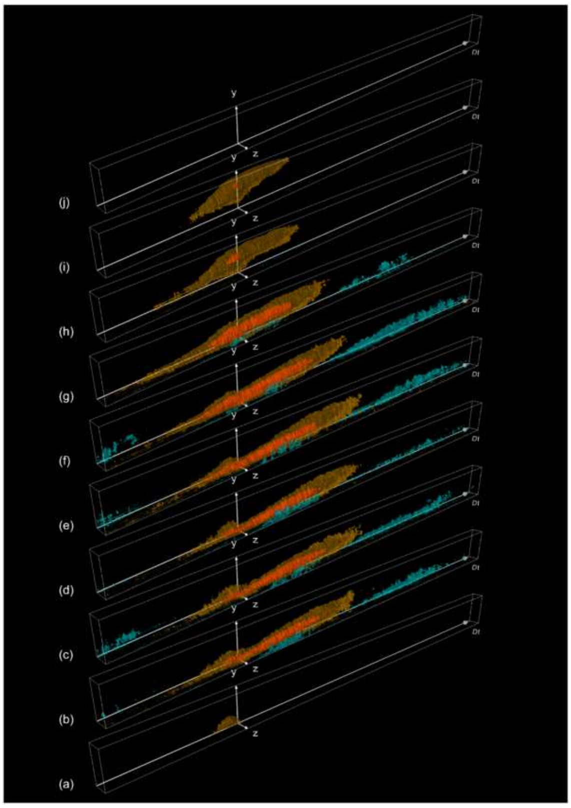

Figure 2. From bottom to top, 3D plots of R_{pu} for pressure reference positions (a) to (j) in table 1 and at Re_θ=10 000.

RESULTS

Because of the limitation of the space, we present only the results at the intermediate Reynolds number Re_θ =10 000 in this paper. The basic statistical characteristics of the boundary layer, e.g., profiles of mean and r.m.s. of velocity, from the present SPIV measurements are in good agreement with the hotwire data obtained in the same facility (Carlier & Stanislas, 2005). The pressure fluctuations exhibits a peak $p'/(\rho U_e^2) = 5.2\times10^{-3}$ at the second measurement location $y^+ = 56$, and the profile of the present measurement at Re_θ =10 000 agrees well with the experimental data in the literature (Tsuji *et al.*, 2007).

Spatio–temporal pressure–velocity correlations

The space–time correlation of the fluctuating pressure and velocity, R_{pu_i} is defined as

$$R_{pu_i}(\Delta t, y, z) = \overline{p(t+\Delta t, y_p, 0)u_i(t, y_p+\Delta y, \Delta z)}$$

where t is the time of stereo PIV recording, y_p is the position of the pressure probe, Δy and Δz are the separation of the moving point along y and z respectively (here $\Delta z = z$ as $z_p = 0$). Since the time-resolved pressure signal is available, the correlation of the velocity field at the time t and the pressure signal around t is evaluated.

Figure 2 shows a 3D representation of the space-time R_{pu} correlation at Re_θ = 10 000 and at the different pressure reference positions given in table 1. In these figures, the range of Δt shown is $-4 \le \Delta t U_e/\delta \le 12$, and the full PIV measurement area is plotted, which is about $\delta \times 0.4\delta$ in y and z directions, respectively. These correlations are normalized everywhere by ρU_e^3. This correlation is the

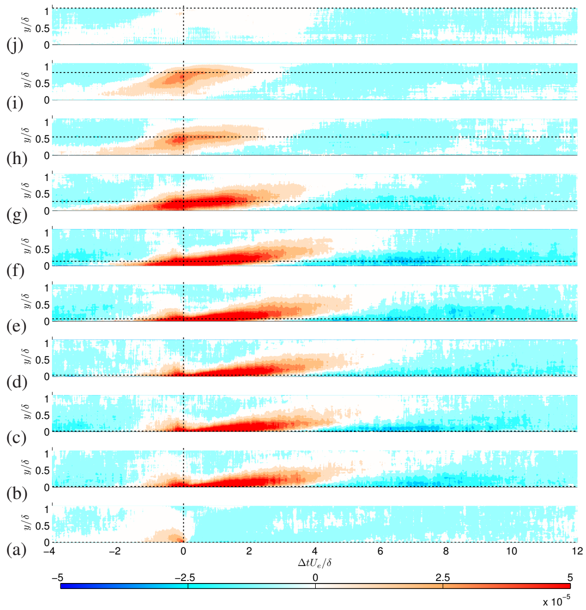

Figure 3. Cuts of R_{pu} in $\Delta t - y$ plane at $z = 0$. The dotted-line indicates the pressure reference position as given in table 1.

most representative of the elongated large scale structures of the boundary layer, as it extends on several boundary layer thicknesses. It has a significant evolution in y by a change of shape. Also, what appears clearly is a strong difference between the correlation with the fixed point at the wall (corresponding to (a) of table 1) which is quite localized and those in the field (b-j) which are extended in time. To look at the correlation structure, a cut in the $z = 0$ plane is done in figure 3, for positions (a-j) of the pressure point as given in table 1. As a difference to the pressure point at the wall, R_{pu}exhibits an inclined elongated shape in Δt for all pressure probe positions except the last (j) one.

Looking in more details at the main positive correlation region, for wall distances smaller than $y_p/\delta \sim 0.1$ (b-e), two characteristic patterns are observed: a small one, which is relatively localized in negative Δt and around the fixed point and a longer one which is inclined and elongated in positive Δt direction with a shallow angle to the horizontal axis. The small region on the negative Δt side is visible from (b) to (f), that is up to about 0.15δ. In this region, for a given Reynolds number, the shape and size of the positive correlation region does not change very much with y. On the positive Δt side, beyond $y_p/\delta \sim 0.1$, the two above distributions building the positive correlation region merge and form one large correlation pattern extending on both positive and negative Δt. This inclined structure shifts progressively toward negative Δt when moving the pressure point away from the wall. The shape of this large positive correlation region changes again significantly beyond y/δ = 0.55 (h), where it starts to disconnect progressively from the wall. While the distributions at other Reynolds numbers are not shown here, it is noted that both the extension and the angle of elongated part show the Reynolds number dependency even when it is scaled with the outer variables.

Figure 4 gives a cut in the $y-z$ plane at $\Delta t U_e/\delta = -0.4$ and characterizes the compact structure on the negative Δt side, when the pressure reference position is closer than $y/\delta \sim 0.1$ to the wall (b-e) the correlation has a relatively

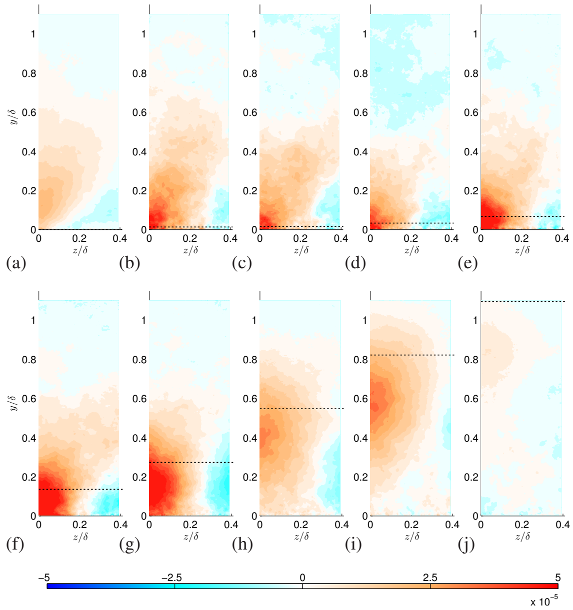

Figure 4. Cuts of R_{pu} in the $y-z$ plane at $\Delta t = -0.4\delta/U_e$. The dotted-line indicates the pressure reference position as given in table 1.

isotropic shape in the (y,z) plane, with a center at the wall and a size of the order of 0.2 δ, whatever the reference point is. A significant difference with the pressure point at the wall is that, in the field, the correlation extends along the wall. When the pressure point moves further away from the wall ($y/\delta \geq 0.1$) (f-j), the correlation tends to spread toward the wall in a more and more asymmetric way (f-g) before it separates from it (h-i) and disappears (j). This corresponds in figure 3 to the stage when the downstream elongated structure, moving upstream overrides the wall structure. For the reference point at $y/\delta = 0.82$ (i), the correlation exhibits its peak around $y/\delta = 0.64$ and spreads within $0.1 \leq y/\delta \leq 1.0$.

The second correlation of interest is the R_{pv} space-time correlation of pressure and wall-normal velocity. A cut through it in the $\Delta t - y$ plane at $z = 0$ is given in figure 5. The correlation is significantly weaker than R_{pu}, but this is not surprising as the wall normal velocity fluctuations are known to be smaller than streamwise ones. For the pressure reference position close to the wall (b-e), the R_{pv} correlation has a shape which is very similar to that with the pressure point at the wall (a): a positive lobe on the positive Δt side and a negative lobe on the negative Δt side, both at an angle which is roughly 45°. Besides that an elongated region of negative correlation develops close to the wall on the positive Δt side. This region has a time extension of the order of $2.5\delta/U_e$. In the outer part, the positive correlation fades rapidly away with increasing y_p. The negative lobe becomes more isotropic and separates from the wall, with an intensity which goes decreasing toward the edge of the boundary layer where it disappears. The negative elongated region grows in size, separates also from the wall and decreases in intensity much faster than the previous one to disappear around 0.8δ. Based on what was observed for the previous R_{pu} correlation, it seems quite natural to associate the two antisymmetric lobes observed in the inner layer to the compact structure of the R_{pu} correlation (they are of comparable size) and the elongated negative struc-

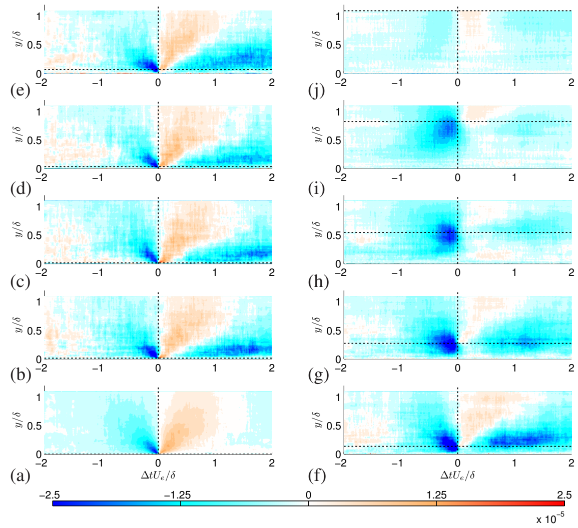

Figure 5. Cuts of the R_{pv} in $\Delta t - y$ plane at $z = 0$. The dotted-line indicates the pressure reference position as given in table 1.

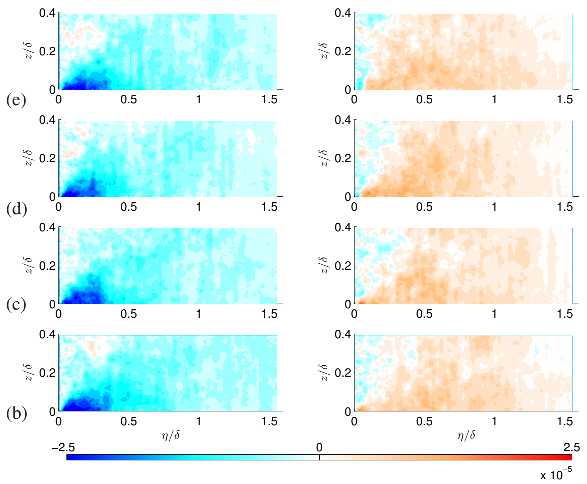

Figure 6. Cuts in the $z-\eta$ plane of the negative (left) and positive (right) lobes of the R_{pv} correlation. Pressure reference position as given in table 1.

ture to the positive one observed at the same place in the R_{pu} plots, but with a longer time extent of $5\delta/U_e$ at this Reynolds number.

In order to estimate the spanwise extent of the two lobes, Figure 6 shows for points (b) to (e) cuts in the $z-\eta$ plane, where η is the coordinate along the crest of each lobe in the $y-\Delta t$ plane. As can be observed, the size and shape of the lobes are very similar in the whole inner region and comparable between positive and negative lobes. Taking into account the symmetry with respect to the $z = 0$ plane, they are about 0.4δ in span and 0.6δ in wall normal extent. In the outer part, the spanwise size of the negative lobe does not change much that is of the order of 0.4δ. It is interesting to note that in this outer region, R_{pv} is more compact and isotropic than R_{pu} but at (h) and (i), it has its maximum at the same location with respect to the fixed point as the positive region of the R_{pu} correlation.

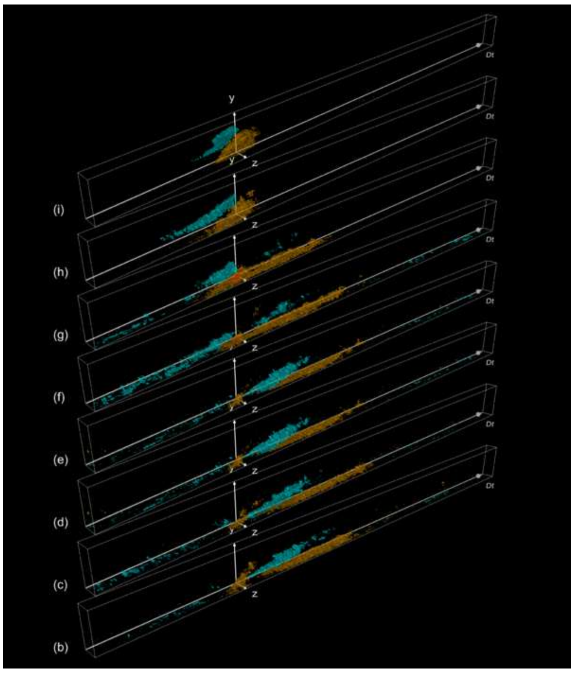

Figure 7. 3D representation of R_{pw} and for the different pressure reference positions as given in table 1.

The last correlation to be analyzed is R_{pw}. As it is zero in the $z = 0$ plane due to homogeneity, it is first plotted in 3D in Figure 7 for the different pressure reference positions and at Reynolds number $Re = 10\ 000$. As a complement, a cut by a $y-\Delta t$ plane at $z = 0.2\delta$ is given in figure 8. This is the most complex correlation among the three as it has several significant correlation regions and shows significant changes both with wall distance. First, based on the previous analysis of R_{pu} and R_{pv}, it is possible here again to distinguish two regions in the correlation. Close to the origin, in the inner part, there is a positive correlation region which is in close similarity to the same correlation with the fixed point at the wall. This can be clearly seen in figure 8 as a S shaped positive correlation region, located close to the origin, on both positive and negative Δt sides, and clearly detectable for the fixed point in the inner part (b-e). This region has its maximum close to the wall but occupies most of the boundary layer thickness. Next, also in the inner part of the boundary layer, a group of two elongated structures, one positive and one negative, appear on the downstream side of the fixed point ($\Delta t > 0$). They obviously work together and are not independent from the elongated structures observed in the other correlations. As this correlation is antisymmetric, this very elongated positive structure could be linked to a meandering motion of the large scales of the boundary layer as it occupies most of its thickness. Besides, the couple of positive and negative elongated region for $\Delta t U_e/\delta < 4$ is clearly indicative of streamwise oriented vortical motions. In the outer part, the wall structure disappears first (f). The elongated structures are still visible in (f-g) but fading. A new structure starts to be clearly visible in (f) with an elongated negative correlation region and extending far upstream in negative Δt and a small positive correlation around the fixed point, obviously coupled to the negative one and laying above it. These two regions grow in wall normal size and compact themselves in time when moving the fixed point toward the boundary layer edge. Looking again at the shape of this outer region structure coupling a positive and negative correlation region, it is strongly evoking an elongated streamwise oriented vortical structure with a size of the order of the boundary layer thickness.

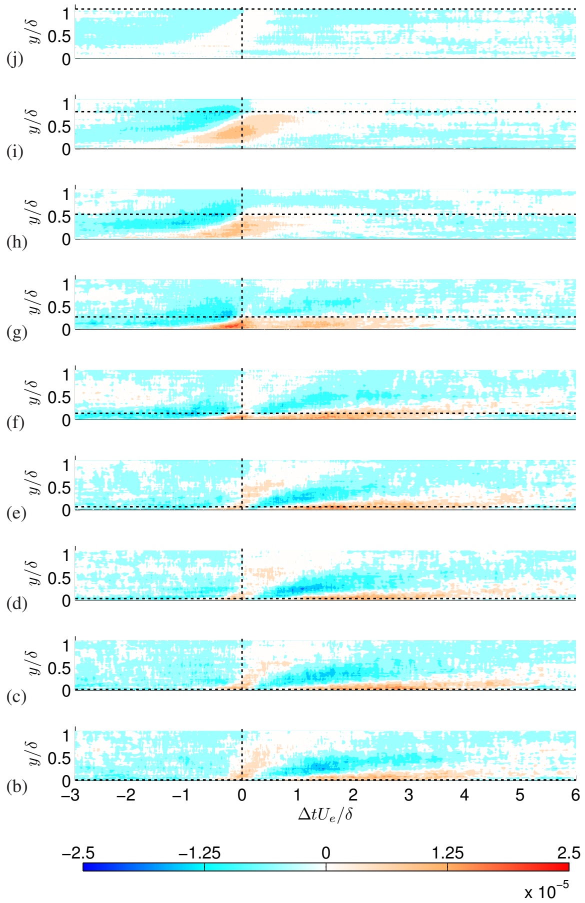

Figure 8. Cuts of the R_{pw} in $\Delta t - y$ plane at $z = 0.2\delta$. The dotted-line indicates the pressure reference position as given in table 1.

In order to assess better the spanwise extent of this correlation, figure 9 shows the $y-z$ cut of R_{pw} at $\Delta t = 0$ and figure 10 the same cut but at $\Delta t = 1.5\delta/U_e$. In figure 9, in the inner layer (b-e), only the inner positive structure is visible. It is strongly inclined toward the wall, not changing very much with the fixed point position and extends beyond the field of view of 0.4δ in z. It goes up to 0.6δ in y and probably 0.5δ in z. In the outer part, the positive part of the outer structure is first visible (f). It is relatively compact and already located below the fixed point in (f). When moving the pressure point outward (g-i), this positive region grows in size, decreases in intensity and does not follow the fixed point upward. A large and weaker negative correlation region forms above it and above the fixed point. It also weakens and moves down with respect to the pressure point when moving it outward.

The cuts at $\Delta t = 1.5\delta/U_e$ given in figure 10 show a completely different picture. For the fixed point in the inner region (b-e) the positive correlation close to the wall has a nearly constant thickness of the order of 0.15δ, but a spanwise extent a bit larger than 0.4δ. It is ridden on a wide region of negative correlation of comparable intensity, but reaching 0.6δ along y and difficult to scale along z (it is much larger than the field of view). Both regions take off

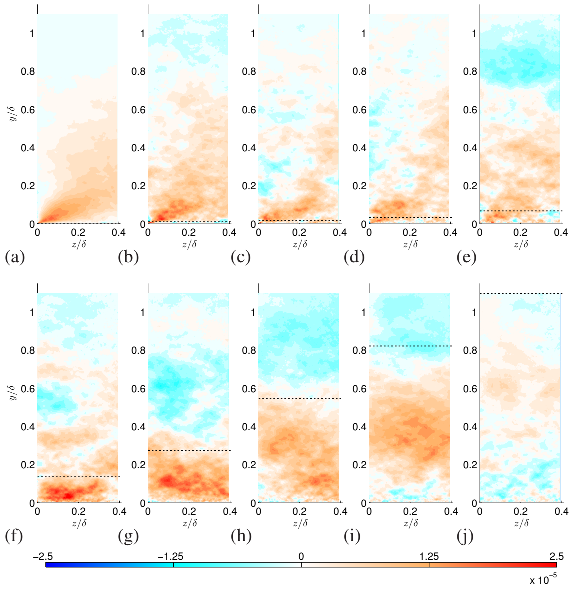

Figure 9. Cuts of R_{pw} in the $y-z$ plane at $\Delta t = 0$ for the different pressure reference positions as given in table 1.

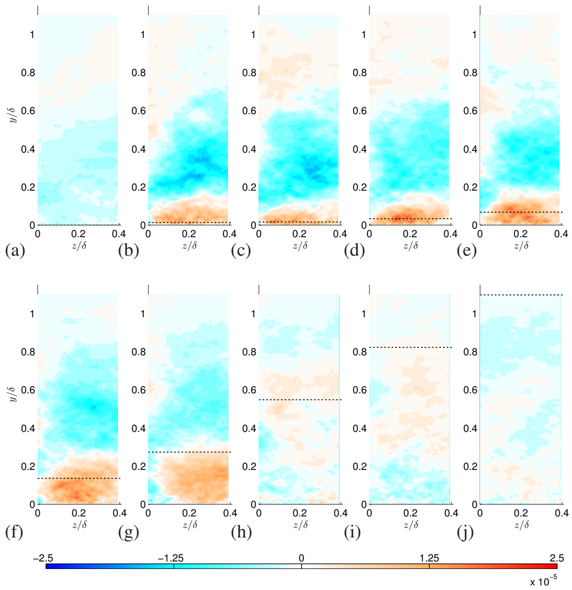

Figure 10. Cuts of R_{pw} in the $y-z$ plane at $\Delta t = 1.5\delta/U_e$ for the different pressure reference positions as given in table 1.

from the wall when increasing the fixed point distance (f-g) and disappear rapidly (h-j). It is interesting to note here that in the pressure creating events, a positive w motion in the inner region is associated to a negative one in the outer region and vice-versa.

CONCLUSION

The 3D space-time pressure-velocity correlations in a turbulent boundary layer have been investigated by simultaneous measurements of the fluctuating pressure and the three velocity components. For the pressure-streamwise velocity correlations, two structures having different streamwise extension are observed. One is compact, located upstream of the pressure event and which acts mostly in the inner part of the boundary layer and at the wall. The second one occupies the whole boundary layer thickness, is elongated with a significant extent and inclined to the wall at a shallow angle. The pressure-wall normal velocity correlation at the pressure reference position $y_p < 0.1\delta$ is symmetric about $\Delta t = 0$: positive and negative lobes lie with an extension of 0.3δ inclined at about $45°$. In the pressure-spanwise velocity correlation, the structures with short and long extensions are recognized like R_{pu}. The pattern of the correlation in the outer part of the boundary layer can be related to the streamwise vortical structures with the size of the boundary layer thickness and its meandering.

ACKNOWLEDGEMENT

We are thankful to the “Conseil Régional Nord Pas de Calais” for providing a fellowship to Y. Naka which allowed to perform this experiment. We are also thankful to CISIT for financial support.

REFERENCES

Adrian, R. J. 2007 Hairpin vortex organization in wall turbulence. *Phys. Fluids* **19** (4), 041301.

Carlier, J. & Stanislas, M. 2005 Experimental study of eddy structures in a turbulent boundary layer using particle image velocimetry. *J. Fluid Mech.* **535**, 143–188.

Coudert, S. & Schon, J. P. 2001 Back projection algorithm with misalignment corrections for 2D3C stereoscopic PIV. *Meas. Sci. Technol.* **12**, 1371–1381.

Foucaut, J.-M., Coudert, S., Stanislas, M. & Delville, J. 2011 Full 3D correlation tensor computed from double field stereoscopic PIV in a high Reynolds number turbulent boundary layer. *Exp. Fluids* **50** (4), 839–846.

Hutchins, N. & Marusic, I. 2007 Evidence of very long meandering features in the logarithmic region of turbulent boundary layers. *J. Fluid Mech.* **579**, 1–28.

Kovasznay, L. S. G., Kibens, V. & Blackwelder, R. F. 1970 Large-scale motion in the intermittent region of a turbulent boundary layer. *J. Fluid Mech.* **41**, 283–325.

Naka, Y., Omori, T., Obi, S. & Masuda, S. 2006 Simultaneous measurement of fluctuating velocity and pressure in a turbulent mixing layer. *Int. J. Heat Fluid Fl.* **27**, 737–746.

Soloff, S., Adrian, R. J. & Liu, Z-C. 1997 Distortion compensation for generalized stereoscopic particle image velocimetry. *Meas. Sci. Technol.* **8**, 1441–1454.

Tsuji, Y., Fransson, J. H. M., Alfredsson, P. H. & Johansson, A. V. 2007 Pressure statistics and their scaling in high-Reynolds-number turbulent boundary layers. *J. Fluid Mech.* **585**, 1–40.

Tutkun, M., George, W. K., Delville, J., Stanislas, M., Johansson, P. B. V., Foucaut, J.-M. & Coudert, S. 2009 Two-point correlations in high Reynolds number flat plate turbulent boundary layers. *J. Turbul.* **10**.

Willert, C. 1997 Stereoscopic digital image velocimetry for applications in wind tunnel flows. *Meas. Sci. Technol.* **8**, 1465–1479.